

## Basic physics of Alfvén instabilities driven by energetic particles in toroidally confined plasmas<sup>a)</sup>

W. W. Heidbrink<sup>b)</sup>

*Department of Physics and Astronomy, University of California, Irvine, Irvine, California 92697, USA*

(Received 16 November 2007; accepted 4 January 2008; published online 15 February 2008)

Superthermal energetic particles (EP) often drive shear Alfvén waves unstable in magnetically confined plasmas. These instabilities constitute a fascinating nonlinear system where fluid and kinetic nonlinearities can appear on an equal footing. In addition to basic science, Alfvén instabilities are of practical importance, as the expulsion of energetic particles can damage the walls of a confinement device. Because of rapid dispersion, shear Alfvén waves that are part of the continuous spectrum are rarely destabilized. However, because the index of refraction is periodic in toroidally confined plasmas, gaps appear in the continuous spectrum. At spatial locations where the radial group velocity vanishes, weakly damped discrete modes appear in these gaps. These eigenmodes are of two types. One type is associated with frequency crossings of counterpropagating waves; the toroidal Alfvén eigenmode is a prominent example. The second type is associated with an extremum of the continuous spectrum; the reversed shear Alfvén eigenmode is an example of this type. In addition to these normal modes of the background plasma, when the energetic particle pressure is very large, energetic particle modes that adopt the frequency of the energetic particle population occur. Alfvén instabilities of all three types occur in every toroidal magnetic confinement device with an intense energetic particle population. The energetic particles are most conveniently described by their constants of motion. Resonances occur between the orbital frequencies of the energetic particles and the wave phase velocity. If the wave resonance with the energetic particle population occurs where the gradient with respect to a constant of motion is inverted, the particles transfer energy to the wave, promoting instability. In a tokamak, the spatial gradient drive associated with inversion of the toroidal canonical angular momentum  $P_\zeta$  is most important. Once a mode is driven unstable, a wide variety of nonlinear dynamics is observed, ranging from steady modes that gradually saturate, to bursting behavior reminiscent of relaxation oscillations, to rapid frequency chirping. An analogy to the classic one-dimensional problem of electrostatic plasma waves explains much of this phenomenology. EP transport can be convective, as when the wave scatters the particle across a topological boundary into a loss cone, or diffusive, which occurs when islands overlap in the orbital phase space. Despite a solid qualitative understanding of possible transport mechanisms, quantitative calculations using measured mode amplitudes currently underestimate the observed fast-ion transport. Experimentally, detailed identification of nonlinear mechanisms is in its infancy. Beyond validation of theoretical models, the future of the field lies in the development of control tools. These may exploit EP instabilities for beneficial purposes, such as favorably modifying the current profile, or use modest amounts of power to govern the nonlinear dynamics in order to avoid catastrophic bursts. © 2008 American Institute of Physics. [DOI: 10.1063/1.2838239]

### I. INTRODUCTION

Alfvén waves that are driven unstable by superthermal energetic particles (EP) are common in both natural and laboratory plasmas. The topic is of interest from a fundamental scientific perspective and for the practical realization of fusion energy. From a scientific perspective, the nonlinear dynamics of Alfvén instabilities occupies an interesting regime where kinetic and magnetohydrodynamic (MHD) nonlinearities can both be important. (In particle accelerators, the former dominates while, in fluid dynamics, MHD-like nonlinearities dominate.) From a practical perspective, transport of fusion reaction products in a reactor will impact device performance, while significant losses could be catastrophic.

Indeed, in early studies of toroidal Alfvén eigenmodes (TAE) in tokamaks, over 50% of the beam power was lost and beam ions expelled by TAEs ablated material from protective tiles on the outer wall, coating optical elements with graphite.<sup>1</sup> In another experiment, fast ions that were accelerated by ion cyclotron heating were transported by TAEs onto orbits that were trapped in ripple wells produced by the toroidal field coils; these fast ions bored a hole in a vacuum port, venting the machine to atmosphere.<sup>2</sup>

This is not the first review paper on this topic. In 1999, Wong reviewed experimental results;<sup>3</sup> his paper is comprehensive and is the best available summary of Tokamak Fusion Test Reactor (TFTR) measurements. A lengthy theoretical review appeared in 1999;<sup>4</sup> recently several less comprehensive theoretical reviews have also appeared.<sup>5-7</sup> A comprehensive review of fast-ion data in tokamaks through

<sup>a)</sup>Paper XR1 1, Bull. Am. Phys. Soc. **52**, 349 (2007).

<sup>b)</sup>Invited speaker.

1993 appears in Ref. 8, but the material on Alfvén instabilities is dated. A more recent but less exhaustive overview of energetic ion effects in tokamaks was published in 2004.<sup>9</sup> Another general resource on fast-ion behavior is the ITER Physics Basis.<sup>10,11</sup> Key issues in burning plasmas are highlighted in Ref. 12. For a clear exposition of the theoretical fundamentals, the best available document is the first four chapters of Pinches' thesis.<sup>13</sup> For the theory of fast-ion transport, White's textbook<sup>14</sup> is a useful resource.

The goal of this paper is to provide a conceptual overview of the field. As much as possible, topics are explained in general physics language at a level accessible to an uninitiated graduate student. Citations are selective, with clarity rather than priority as the primary criterion. The phenomenon of Alfvén eigenmodes is discussed first (Sec. II), followed by a discussion of EP orbits, wave-particle resonance, and energy transfer (Sec. III). Section IV introduces the distinction between normal modes and energetic particle modes (EPM). Next, nonlinear dynamics are considered (Sec. V). The final section surveys the field's frontier: control tools for EP-driven instabilities.

## II. ALFVÉN GAP MODES

Shear Alfvén waves are transverse low frequency electromagnetic waves that propagate along the magnetic field  $\mathbf{B}$ . When the wave frequency  $\omega$  is small compared to the ion cyclotron frequency  $\Omega_i$  and when kinetic effects are unimportant, the dispersion relation in a uniform field is simply

$$\omega = k_{\parallel} v_A, \quad (1)$$

where  $k_{\parallel}$  is the wave vector in the direction of the magnetic field and

$$v_A = B / \sqrt{\mu_0 \sum n_i m_i} \quad (2)$$

is the Alfvén speed. Here,  $\sum n_i m_i$  is the mass density of the plasma. Through quasineutrality, in plasmas dominated by species of the same charge-to-mass ratio  $Z_i/A_i$ , the mass density is linearly proportional to the electron density  $n_e$ , so  $v_A \propto B/\sqrt{n_e}$ . The transverse polarization of shear Alfvén waves implies that the parallel components of the electric and magnetic fields  $\tilde{E}_{\parallel}$  and  $\tilde{B}_{\parallel}$  are much smaller than the transverse components  $\tilde{E}_{\perp}$  and  $\tilde{B}_{\perp}$ , i.e.,  $\tilde{E}_{\parallel} \ll \tilde{E}_{\perp}$  and  $\tilde{B}_{\parallel} \ll \tilde{B}_{\perp}$ . The simple dispersion relation [Eq. (1)] implies that the group velocity  $\partial\omega/\partial\mathbf{k}$  equals the phase velocity  $\omega/k_{\parallel}\hat{b}$ , so low frequency shear Alfvén waves in uniform plasma are dispersionless. (Here  $\hat{b}$  represents a unit vector in the direction of the magnetic field.) Physically, shear Alfvén waves are analogous to transverse waves on a plucked string, with the tension ( $\propto B^2$ ) being supplied by the magnetic field and the mass density being supplied by the ions.

When excited by drawing an axial current to a disk, the observed properties of shear Alfvén waves in a straight cylinder agree well with this simple description (with kinetic effects taken into account).<sup>15</sup> The uniform field is in the axial direction  $\hat{z}$ , the wave electric field is in the radial direction  $\hat{r}$ , and the wave magnetic field is in the azimuthal direction  $\hat{\theta}$ . The situation changes if there is an azimuthal component to

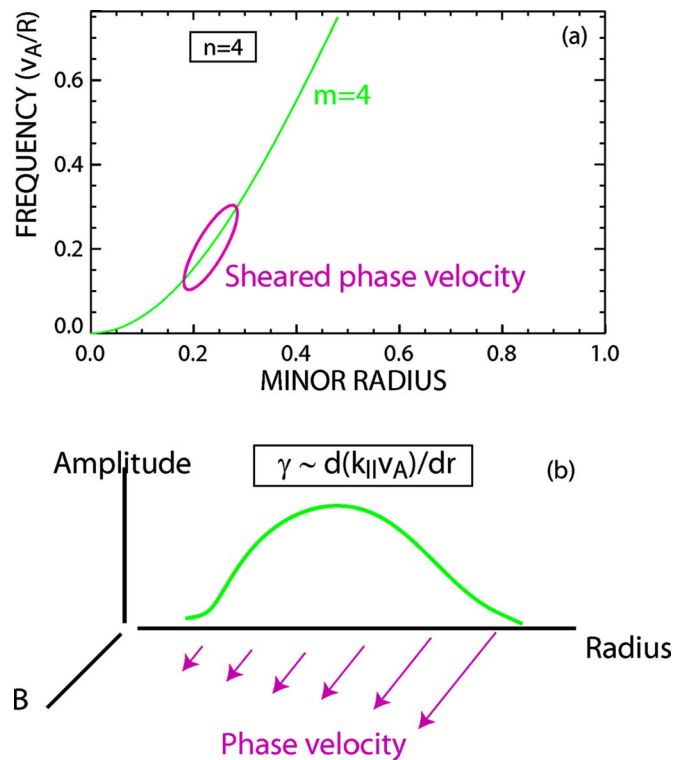


FIG. 1. (Color online) (a) Dispersion relation for an  $m=4$ ,  $n=4$  wave in a cylindrical plasma. The phase velocity is a strong function of radial position. (b) A hypothetical disturbance launched in the highlighted region. The pulse will rapidly disperse and shear.

the ambient magnetic field configuration, however. Now the azimuthal component of the parallel wavelength must be periodic. Similarly, if there is a periodicity constraint in the axial direction, as there is in the toroidal counterpart of a cylinder, the wavelength must also be periodic. The corresponding integer mode numbers are generally represented by  $m$  in the azimuthal (poloidal) direction and by  $n$  in the axial (toroidal) direction. If the field line rotates azimuthally  $1/q$  times in the axial periodicity length  $2\pi R$ , these periodicity constraints require that  $k_{\parallel} = (n - mq)/R$ , where  $q$  is the familiar safety factor used in tokamak research. The safety factor is usually a function of radius, implying that, in contrast to the uniform field case, the dispersion relation [Eq. (1)] is a function of radius in a sheared magnetic field. Waves that satisfy this dispersion relation are part of the Alfvén continuum.

It is difficult to excite instabilities in the Alfvén continuum. Consider a hypothetical wave packet of finite radial extent [Fig. 1(b)]. Waves at different radii have different velocities [Fig. 1(a)], so the pulse rapidly disperses. The associated damping rate  $\gamma$  is proportional to the gradient of the phase velocity,  $\gamma \propto d/dr(k_{\parallel} v_A)$ . Usually, energetic particles cannot deliver enough energy to the wave to overcome this continuum damping.

There are gaps in the continuous spectrum, however, and the most easily excited modes reside in these frequency gaps. The existence of frequency gaps is a generic wave phenomenon observed in countless physical systems. Familiar examples include the electron band gap in conductors and

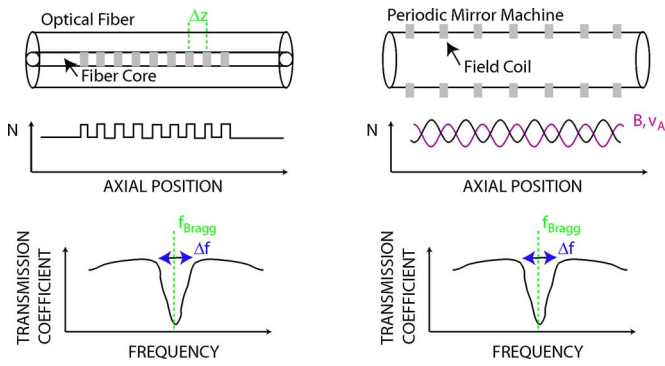


FIG. 2. (Color online) Comparison of an optical fiber with a transmission gap for visible light and a plasma with a transmission gap for shear Alfvén waves. The fiber has a periodically modulated index of refraction in its core. The plasma has a variable magnetic field that results in periodic modulation of the index of refraction  $N$ . The spatial period of the modulations is  $\Delta z$ . Both systems have a propagation gap at the Bragg frequency and the width of the propagation gap  $\Delta f$  is proportional to the amplitude of modulation of  $N$ .

Bragg reflection in optical interference filters. As Lord Rayleigh realized,<sup>16</sup> any periodic modulation of the index of refraction  $N$  will introduce a band gap. In conductors, the periodic changes in potential associated with the ion lattice are associated with periodic changes in  $N$  in the electron wave equation. In photonic crystals, alternating stacks of materials of different  $N$  produce the frequency gap. In optical fibers, periodic variation of the index of refraction of the core produces a “fiber Bragg grating” (Fig. 2). The gap is centered at the Bragg frequency

$$f = \frac{\bar{v}}{2\Delta z}, \quad (3)$$

where  $\bar{v}$  is the average phase velocity and  $\Delta z$  is the distance between the periodically varying elements. In analytic theory, the frequency width of the gap  $\Delta f$  is proportional to the modulation of the index of refraction,  $\Delta f \propto \Delta N$  (for small values of  $\Delta N/\bar{N}$ ). Physically, the gap is caused by destructive interference of counterpropagating waves that reflect off the periodic modulations.

Bragg reflection occurs for Alfvén waves. A periodic magnetic mirror configuration has a frequency gap at the Bragg frequency and the gap width scales with the mirror depth (Fig. 2).<sup>17</sup> Since the Alfvén speed is proportional to  $B$ , the magnetic mirrors cause variations in the index of refraction. Variations in  $B$  are unavoidable in a torus with rotational transform. By Ampère’s law, poloidal currents produce toroidal fields that vary inversely with major radius  $R$ ,  $B \propto R^{-1}$ , so the Alfvén speed inevitably varies along a field line, effectively creating a periodic variation in index of refraction. The poloidal distance around the torus for a field line is  $\Delta z = q2\pi R$ , so Eq. (3) implies that this toroidicity-induced frequency gap is centered at<sup>18</sup>

$$f = \frac{v_A}{2(q2\pi R)} = \frac{v_A}{4\pi qR}. \quad (4)$$

The width of the gap depends on the variation in field strength,  $B_{\max}/B_{\min} \propto (R+r)/(R-r) \approx 1+2r/R$ , so the gap

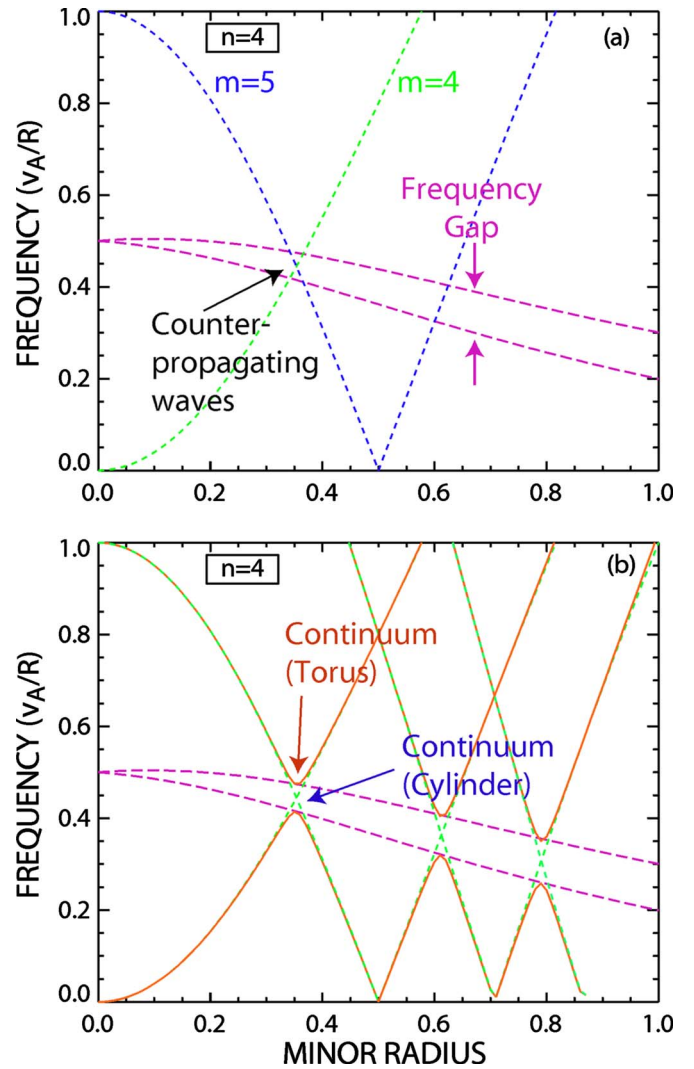


FIG. 3. (Color online) (a) Dispersion relation of two waves with toroidal mode number  $n=4$  and poloidal harmonics of  $m=4$  and  $m=5$  in a plasma with a  $q$  profile that increases monotonically with radius. Frequencies are plotted as positive for both signs of  $k_{\parallel}$ . The frequency gap increases with radius because  $r/R$  increases, which increases the modulation of  $N$ . The two waves are counterpropagating in the frequency gap. (b) Dispersion relation with (solid) and without (dashed) toroidal coupling of the waves. The  $m=6$  and  $m=7$  waves are also shown and intersect at larger radii. Based on Ref. 19.

width, which is proportional to  $\Delta B/\bar{B}$ , is proportional to the inverse aspect ratio  $\epsilon = r/R$ . (Here  $r$  is the minor radius of the torus.)

The previous discussion applies to a field line at any radius in the plasma. In general,  $v_A$ ,  $q$ , and the inverse aspect ratio are all functions of minor radius. Figure 3 illustrates the variation of the toroidicity-induced frequency gap with minor radius for typical tokamak parameters. The center of the gap [Eq. (4)] varies with radius since  $v_A/q \propto 1/q\sqrt{n_e}$  varies with radius. The width of the gap increases with radius because  $\Delta B$  increases as  $r/R$  increases.

Any periodic variation in Alfvén speed produces a frequency gap. Examples that are important in practice include the gap caused by geodesic curvature of the field lines in a finite beta plasma,<sup>20</sup> gaps caused by elongation<sup>18,21</sup> or trian-

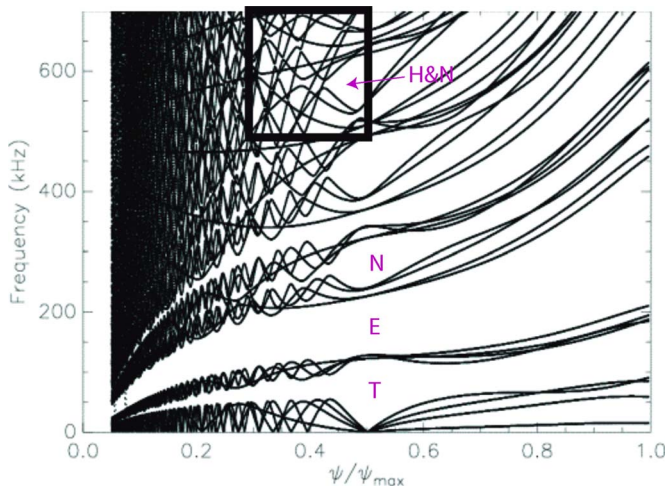


FIG. 4. (Color online) Calculated Alfvén gap structure for an experimental stellarator equilibrium. The “T” (toroidicity), “E” (ellipticity), and “N” (non-circularity) induced gaps are labeled. In the region marked with the bold square, the gaps are caused by both “N” and “H” helicity-induced modulations. Adapted from Ref. 25.

gularity of flux surfaces,<sup>22</sup> and gaps caused by helicity<sup>23</sup> and periodic mirroring in stellarators.<sup>24</sup> The gap structure for actual equilibria are often quite complex (Fig. 4).

Frequency gaps are important because radially extended, weakly damped modes that are not subject to continuum damping can exist in these gaps. Once again, the existence of gap modes is a generic wave phenomenon. In conductors, gap modes are associated with defects in the periodic ionic lattice. In a particularly clear demonstration of gap modes, drilling a hole in a periodic stack of materials of alternating index of refraction creates an eigenmode in the frequency gap.<sup>26</sup> For an eigenmode to exist, the defect must create an effective potential well that localizes the wave. Mathematically, in the absence of a defect, the mode amplitude increases exponentially in the frequency gap. With a potential well, the amplitude remains finite and a mode with vanishing radial group velocity resides in the gap.

Imagine trying to excite Alfvén modes with an external antenna of variable frequency, a situation readily implemented in both experiment and computation. If the antenna frequency intersects the continuum, the wave has a very narrow mode structure [Fig. 5(a)]. In the MHD model, the mode structure is singular; in experiment and more realistic computational models, the wave is strongly damped by interaction with thermal plasma, so the amplitude of the excited wave is small. In contrast, if the antenna frequency coincides with the frequency of a gap mode, the mode structure is regular and spatially extended [Figs. 5(b) and 5(c)]; even with modest antenna currents, these modes can reach amplitudes that are experimentally observable.

Shear Alfvén eigenmodes can be divided into two classes. In the most easily understood case, the radial variation vanishes because of an extremum in the frequency of the continuous spectrum [Fig. 5(b)]. An example is the reversed shear Alfvén eigenmode (RSAE) that occurs in tokamak plasmas with a minimum in the  $q$  profile. At this surface, the radial variation  $\partial\omega/\partial r$  vanishes. An effective potential well

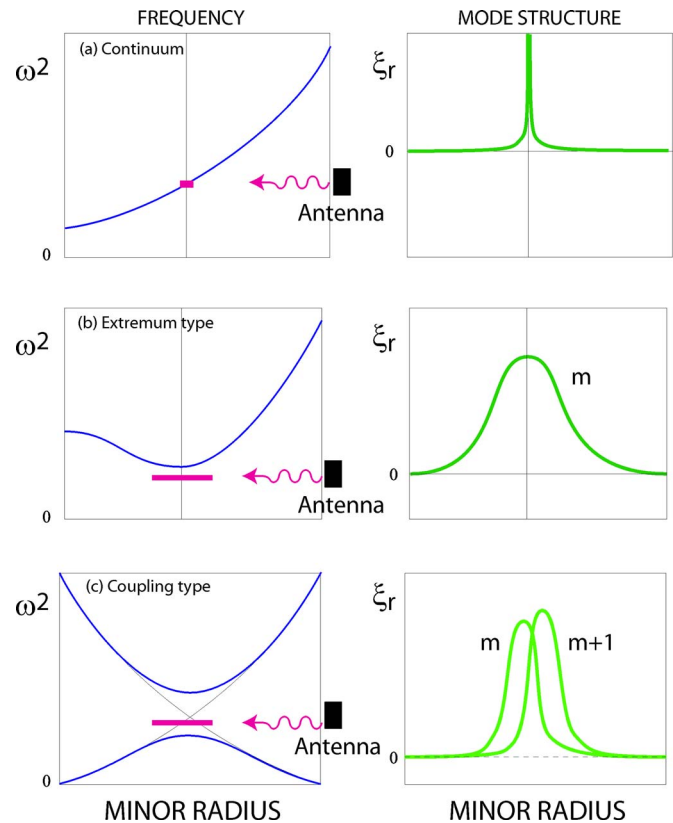


FIG. 5. (Color online) Frequency (left) and mode structure (right) for three different types of Alfvén waves. The waves are excited by an antenna at the edge of the plasma. (a) A continuum wave has a very narrow mode structure that is strongly damped. (b) If the plasma profiles create an extremum in the Alfvén continuum, the antenna may excite a gap mode that is located near the extremum; this wave has (predominately) a single poloidal harmonic. (c) The antenna can also excite gap modes near the extrema created by mode coupling; in this case, the poloidal harmonics of the coupled waves appear. Adapted from Ref. 13.

exists that traps the wave.<sup>27</sup> The mode that resides in this potential well has a single toroidal and poloidal mode number. An example of the experimentally measured mode structure is shown in Fig. 6. The mode resides near the minimum of the measured  $q$  profile and has a frequency that is above

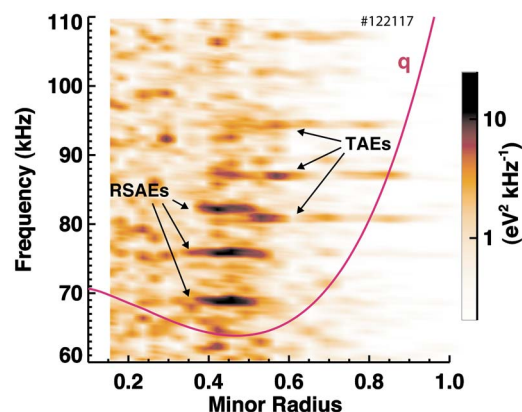


FIG. 6. (Color online) Radial profile of electron temperature fluctuations as measured in the DIII-D tokamak. The  $q$  profile is also shown. RSAEs with different toroidal mode numbers are located near  $q_{\min}$ . More globally extended TAEs are also observed. Adapted from Ref. 28.

the continuum frequency, thus avoiding strong continuum damping. In this case, the “defect” that localizes the eigenmode is the absence of magnetic shear at  $q_{\min}$ .

As the  $q$  profile changes in the plasma, the frequency of the RSAE changes to remain just above the Alfvén continuum at the radius of minimum  $q$ . Experimentally,  $q_{\min}$  usually decreases with time and the modes usually first appear when  $q_{\min}$  crosses a rational integer value. The parallel wave vector is  $k_{\parallel} = |m/q_{\min} - n|/R$ , so the wave frequency gradually rises as  $q_{\min}$  steadily drops. The characteristic appearance of several RSAEs at rational  $q_{\min}$  values (dubbed the “Alfvén cascade”) is quite useful for diagnosis of the evolution of the  $q$  profile.<sup>29</sup>

The second class of gap modes is associated with frequency crossings between counterpropagating waves [Fig. 5(c)]. The most important of these is the TAE. Consider the continuous spectrum of two azimuthal (poloidal) modes with mode number  $m$  and  $m+1$  that have the same axial (toroidal) mode number  $n$  [Fig. 3(a)]. The frequencies of the continuum modes cross at the radius where the parallel wavenumbers have the same absolute value. At this location, one mode is propagating in the positive direction with wavenumber  $k_{\parallel} = n/R - m/qR$  and the other mode is propagating in the negative direction with  $k_{\parallel} = -|n/R - (m+1)/qR|$ . At  $q = (m+1/2)/n$  the magnitude of these wavenumbers is  $|k_{\parallel}| = n/2R$ . The corresponding frequency  $\omega = |k_{\parallel}|v_A = v_A/2qR$  corresponds with the Bragg frequency in the center of the gap [Eq. (4)]. When toroidal coupling is included in the MHD equations, these two waves mix and the frequency crossing is avoided [Fig. 3(b)].<sup>30,31</sup> Avoidance of the frequency crossing creates effective extrema in the continuous spectra. A discrete eigenmode forms at the location of the frequency crossing. In this case, the “defect” that localizes the TAE is the coupling of poloidal harmonics caused by magnetic shear.

The existence of the TAE is very well established experimentally. Detailed comparisons of the measured eigenfunction with MHD calculations show excellent agreement<sup>28</sup> and the measured mode polarization is consistent with a transverse wave, as expected.<sup>32</sup> Excitation by an antenna that sweeps in frequency shows that a weakly damped normal mode exists at a frequency close to the expected value and that this mode follows the evolution of  $v_A$  as the discharge evolves (Fig. 7).<sup>33</sup> Two-dimensional tomographic reconstruction of the eigenfunction from soft x-ray data shows clearly the expected poloidal structure that arises from coupling of the two poloidal harmonics  $m$  and  $m+1$  [Fig. 8(b)].<sup>34,35</sup> In other discharges, soft x-ray measurements of a global Alfvén eigenmode (GAE), which is an AE that arises from a minimum in the Alfvén continuum,<sup>41,115–118</sup> show only a single poloidal harmonic, as expected [Fig. 8(a)].

In practice, gap modes often consist of many coupled poloidal harmonics,<sup>36</sup> especially in strongly shaped, low-aspect ratio devices.

There is an entire taxonomy of Alfvén eigenmodes, the so-called Alfvén “zoo” (Table I). In addition to the TAE, observed modes that arise from counterpropagating waves include the ellipticity-induced Alfvén eigenmode (EAE),<sup>37</sup> and the noncircularity-induced Alfvén eigenmode (NAE).<sup>38</sup>

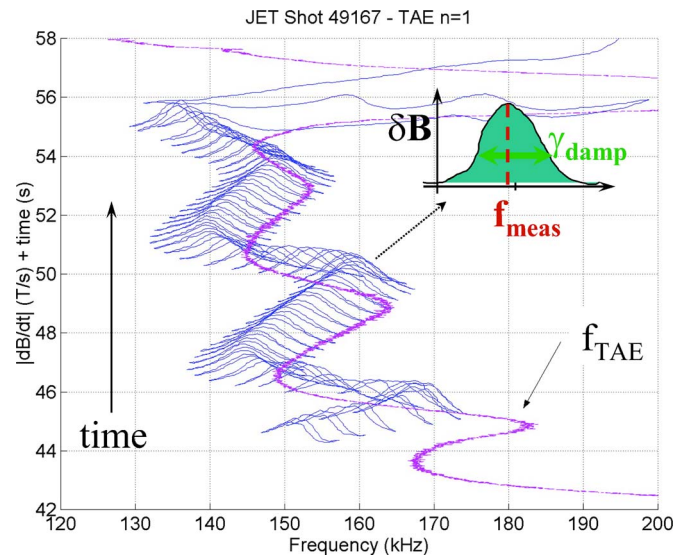


FIG. 7. (Color online) Experimental data from the Joint European Torus (JET) tokamak showing the evolution of the center of the TAE gap (labeled  $f_{\text{TAE}}$ ) and the amplitude of the magnetic field observed as an antenna sweeps its frequency across the gap. A normal mode is excited that exhibits weak damping  $\gamma_{\text{damp}}$  (inferred from the quality factor of the resonance) and follows the evolution of the gap frequency in time. Adapted from Ref. 119.

In stellarators, helicity-induced Alfvén eigenmodes (HAE) (Ref. 39) are also observed. In addition to the RSAE, observed modes that result from an extremum in the Alfvén continuum include the beta-induced Alfvén eigenmode (BAE),<sup>40,36</sup> and GAEs in Ohmic tokamaks,<sup>41</sup> weak-shear stellarators,<sup>35</sup> and (at higher frequency) in spherical tokamaks.<sup>42</sup> Some authors distinguish between TAEs that occur in different pressure limits, such as the core-localized “TAE” in the region of weak shear near the magnetic axis.<sup>43,44</sup> Inclusion of kinetic effects in the theoretical model results in additional modes such as the kinetic TAE (KTAE) at frequencies just above the TAE gap.<sup>45</sup> In addition to these shear Alfvén eigenmodes, there are eigenmodes of the compressional Alfvén wave (CAE),<sup>46</sup> and modes that result from coupling of shear Alfvén waves with acoustic waves, the beta-induced Alfvén acoustic eigenmodes (BAAE).<sup>47</sup> There are subtle differences between the properties of these various modes and definitive observation is controversial in some

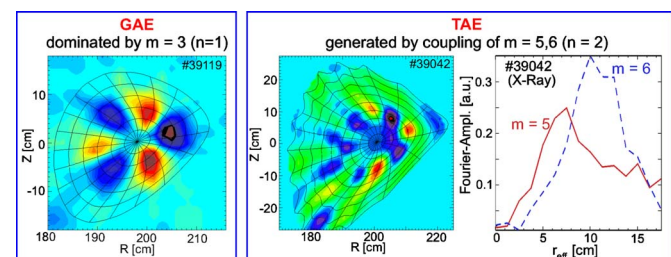


FIG. 8. (Color online) Tomographic reconstructions of soft x-ray fluctuation data obtained on the Wendelstein 7-AS stellarator. The reconstruction on the left is of extremum type, a GAE with a single dominant poloidal harmonic. The reconstruction on the right shows the structure associated with two coupled harmonics ( $m=5$  and  $6$ ); the harmonics interfere constructively on the outside of the device and destructively on the inside. Adapted from Refs. 34 and 35.

TABLE I. Nomenclature of shear Alfvén eigenmodes, listed in ascending (approximately) order of frequency. For coupling-type eigenmodes, the coupled poloidal or toroidal harmonics are given; for extremum-type eigenmodes, the source of the extremum is underlined>. The citations are to the original theoretical and experimental papers.

Acronym	Name	Cause	Theory	Obs.
RSAE <sup>a</sup>	Reversed-shear	$q_{\min}$	[29]	[115]
BAE	Beta	<u>Compressibility</u>	[36]	[40]
GAE <sup>b</sup>	Global	<u>Generic term</u>	[41, 116]	[117]
TAE	Toroidal	$m$ and $m+1$	[30, 31]	[52, 53]
KTAE <sup>c</sup>	Kinetic	Electron dynamics <sup>c</sup>	[66]	[45]
EAE	Ellipticity	$m$ and $m+2$	[22]	[37]
NAE	Noncircularity	$m$ and $m+3$ (or higher)	[22]	[38]
MAE	Mirror	$n$ and $n+1$	[24]	...
HAE	Helicity	$n$ and $m$ combinations	[23]	[39]

<sup>a</sup>Usually in TAE gap but also found in higher-order gaps.

<sup>b</sup>Usually refers to an eigenmode below a minimum in the Alfvén continuum; observed at both low [117] and high [42] frequency.

<sup>c</sup>Electron dynamics discretize the continuum into “kinetic Alfvén waves” (KAW) [118]; these couple to form KTAE. Similarly, KEAE and KHAE exist theoretically.

cases but, like most taxonomy, these details are primarily of interest to the specialist. The basic phenomenon is generic.

### III. ENERGETIC PARTICLE DRIVE

Alfvén waves are driven unstable by the free energy in the EP distribution function. The basic mechanism of destabilization applies to both fast ions and electrons and is applicable to any magnetic configuration. However, in this section, for the sake of clarity, the energetic particles are assumed to be ions in a tokamak. In most cases, generalization to other species and configurations is obvious.

In addition to time  $t$ , it takes six coordinates to describe an arbitrary distribution function: three velocity coordinates and three spatial coordinates. On the time scale of the orbital motion, three quantities are conserved, so only  $6-3=3$  variables are needed to specify a tokamak orbit. Orbits in hot fusion plasmas are completed in a time that is much shorter than characteristic collision times, so one conserved quantity is the energy  $W$ . The rapid gyromotion and the relatively weak variation of  $B$  on the length scale of the gyroradius insure conservation of the magnetic moment  $\mu$ . Finally, in an axisymmetric torus, the canonical toroidal angular momentum  $P_\zeta$  is conserved. The distribution function  $f$  is conveniently described in terms of these three constants of the motion,  $f(W, \mu, P_\zeta; t)$ .

Figure 9 shows a typical EP orbit. The perpendicular velocity causes rapid gyromotion in a plane perpendicular to the field. When the parallel velocity is projected into the poloidal plane, it causes the drift motion to follow flux surfaces. On the other hand, the  $\nabla B$ , curvature, and  $E \times B$  drifts are perpendicular to the field and tend to drive ions away from a confining magnetic surface. In a confinement device, the rotational transform insures that drifts away from the surface are compensated by drifts toward the surface as an ion moves along the magnetic field. Nevertheless, because the  $\nabla B$  and curvature drifts are proportional to the square of

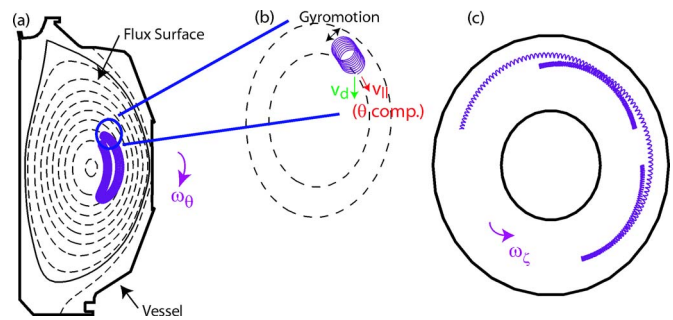


FIG. 9. (Color online) Projection of the orbit of an 80-keV deuterium beam ion in the DIII-D tokamak. (a) Elevation. The dashed lines represent the magnetic flux surfaces. The particle orbits poloidally with a frequency  $\omega_\theta$ . (b) Detail of the beginning of the orbit. The rapid gyromotion, parallel drift along the flux surface, and vertical drift velocity are indicated. (c) Plan view of the orbit. The particle precesses toroidally with a frequency  $\omega_\zeta$ .

the ion velocity, while the parallel motion is linearly proportional to the velocity, the drift orbits of energetic ions often deviate dramatically from flux surfaces. In some cases, the deviations may be so large that the fast ion strikes the wall; this is termed a *loss orbit*. Additionally, for low energy particles there are just two types of orbits (trapped and passing) but, for high energy particles, several other types of orbits exist with names such as “potato.”<sup>14</sup> The complicated orbit phenomenology is most easily described by a diagram in constants-of-motion space that marks topological boundaries between different types of orbits (Fig. 10). The boundaries are important because a wave that moves an ion across a topological boundary causes large radial transport. Energetic ion loss boundaries in tokamaks are well verified experimentally.<sup>8,48</sup>

Power transfer between an ion and a wave requires a nonzero value of  $\mathbf{v} \cdot \mathbf{E}$ . ( $\mathbf{v}$  is the velocity vector and  $\mathbf{E}$  is the electric field of the wave.) For transverse electromagnetic waves like shear Alfvén waves in a uniform field, a particle that travels along the field at the phase velocity “sees” a static magnetic perturbation and no electric field (due to relativistic transformation of the electric field), so the power transfer is zero. In curved fields, power transfer can occur but only the drift velocity  $\mathbf{v}_d$  ultimately contributes. Since the gyromotion is very rapid compared to the mode frequency ( $\Omega_i \gg \omega$ ), the energy transfer associated with the gyromotion  $\oint \mathbf{v}_\perp \cdot \mathbf{E}$  phase averages to zero. A general expression for the power transfer between a particle and the fields of a long-wavelength, low-frequency wave is

$$\frac{dW}{dt} = eZ\mathbf{v}_d \cdot \mathbf{E}_\perp + eZv_\parallel E_\parallel + \mu \frac{\partial B_\parallel}{\partial t}. \quad (5)$$

Here,  $\mathbf{E}_\perp$  is the transverse electric field and  $E_\parallel$  and  $B_\parallel$  are the parallel electric and magnetic fields. Theoretically, the first term is normally considered dominant for shear Alfvén waves. The second term is small for  $\omega \ll \Omega_i$  as long as mode conversion to waves with a large electrostatic component does not occur. The third term is small because the waves are nearly transverse in a low  $\beta$  tokamak, so both  $B_\parallel$  and  $\omega$  are small. Experimentally, the relative importance of these terms awaits confirmation.

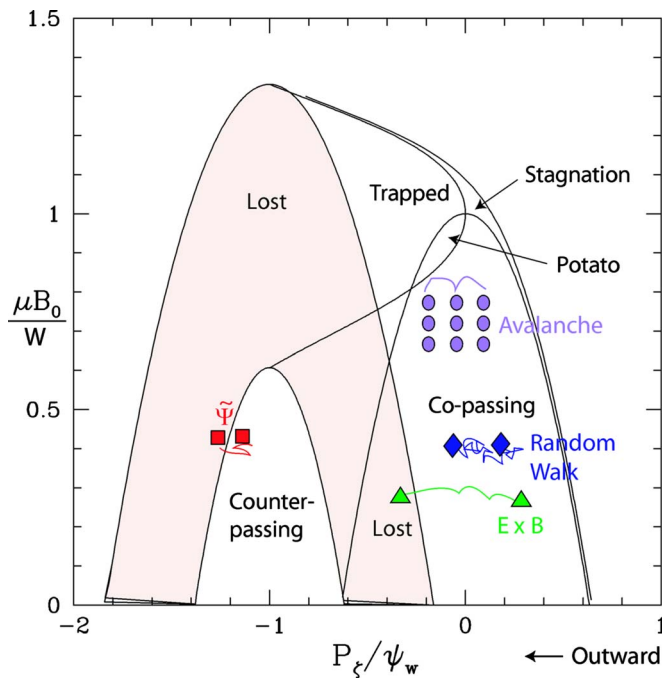


FIG. 10. (Color online) Classification of different orbit types for beam ions in the DIII-D tokamak vs magnetic moment  $\mu$  and canonical angular momentum  $P_\xi$ . The poloidal flux at the wall is  $\Psi_w$ , the particle energy is  $W$ , and the magnetic field at the magnetic axis is  $B_0$ . Particles that move outward from the magnetic axis move leftward on the  $P_\xi$  axis. Four types of EP transport are illustrated. (Red rectangle) The wave can perturb the equilibrium ( $\vec{\Psi}$ ), causing particles near a loss boundary to collide with the wall. (Green triangle) Particles that stay in phase with a mode throughout the plasma can convectively escape via the  $\vec{E} \times \vec{B}$  drift. (Blue diamond) Particles can diffuse as they receive velocity kicks associated with the many wave-particle resonances in the plasma. (Purple circles) If the EPs move outward, they can locally alter the EP gradient and destabilize a new wave that transports them further, where a new wave is destabilized, etc.

Focusing on the power transfer between the drift motion and the transverse electric field, because the growth rate is generally small compared to the wave frequency ( $\gamma \ll \omega$ ), it is convenient to consider the energy transfer after averaging over dozens of orbital cycles. To avoid phase averaging to zero, a harmonic of the drift-orbit frequency must match the wave frequency. All types of orbits are characterized by two frequencies, the frequency of toroidal motion  $\omega_\zeta$  and the frequency of poloidal motion  $\omega_\theta$  (Fig. 9). For the orbit and wave phases to match after many cycles, the following condition must be satisfied:

$$\omega + p\omega_\theta - n\omega_\zeta \approx 0, \quad (6)$$

where  $p$  is an integer. Though necessary, this condition alone does not guarantee net energy transfer. The relevant quantity is  $\oint \mathbf{v}_d \cdot \mathbf{E}_\perp$  over many complete orbital cycles. To evaluate this term, it is convenient to express  $\mathbf{v}_d$  and  $\mathbf{E}_\perp$  in terms of poloidal angle. The drift velocity is written as a Fourier series in  $\theta$  harmonics,

$$\mathbf{v}_d = \sum_{l=\pm 1, \pm 2, \dots} A_l e^{il\theta}, \quad (7)$$

where the  $A_l$  are Fourier coefficients. For low energy particles in a circular cross-section tokamak, only the  $l = \pm 1$

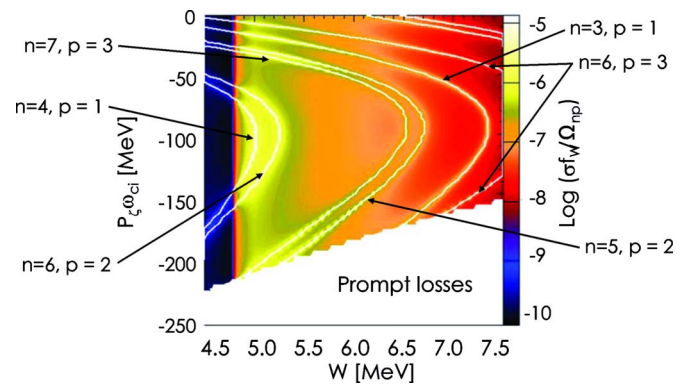


FIG. 11. (Color online) Calculated resonances for rf-accelerated tail ions in the JET tokamak in the energy/toroidal-angular-momentum plane. The toroidal ( $n$ ) and poloidal ( $p$ ) values of the resonances are labeled. The amplitude scale takes into account the probability of detection by a gamma-ray diagnostic. Adapted from Ref. 51.

terms are appreciable; however, in strongly shaped plasmas and for large drift-orbit displacements, higher order harmonics are also important. The resonance condition for nonzero  $\oint \mathbf{v}_d \cdot \mathbf{E}_\perp$  is

$$\omega + (m+l)\omega_\theta - n\omega_\zeta \approx 0. \quad (8)$$

Resonant energy transfer can take place with all of the poloidal harmonics that comprise the gap mode.

As a simple example, consider TAE resonance with passing fast ions that circulate in the direction of the field line. The toroidal circulation frequency is  $\omega_\zeta = v_\parallel / R$  and the poloidal circulation frequency is  $\omega_\theta = v_\parallel / qR$ . Using the facts that  $\omega = v_A / 2qR$  [Eq. (4)] and that the mode is centered at the frequency crossing at  $q = (m+1/2)/n$ , Eq. (8) implies that  $|l|=1$  resonance occurs when  $v_\parallel = v_A$  and  $v_\parallel = v_A/3$ . For co-going particles, one resonance is with the  $m$  harmonic and another is with the  $m+1$  harmonic that interfere constructively to form the TAE. Equation (8) implies and computer simulations<sup>49</sup> verify that both co- and counter-circulating particles can resonate with the mode. (The assertion that counter-circulating ions do not interact with a mode that rotates in the ion-diamagnetic direction in Refs. 3 and 50 is incorrect.)

For other gap modes, the fundamental  $|l|=1$  resonances are different. For example, for the EAE with  $\omega = v_A / qR$ , the  $m$  and  $m+2$  modes couple at the  $q = (m+1)/n$  surface, so circulating particles with  $v_\parallel = v_A/2$  resonate with the mode.<sup>38</sup>

In practice, higher  $l$  harmonics often are important too. Figure 11 shows the many resonances between a high-energy ion-cyclotron accelerated fast ion population and the observed TAEs in a JET tokamak plasma. Experimentally, an enormous number of different EP populations have driven unstable Alfvén gap modes through a wide variety of different resonances. Neutral beams,<sup>52,53</sup> ion-cyclotron accelerated fast ions,<sup>54</sup> alpha particles produced in deuterium-tritium (D-T) fusion reactions,<sup>44</sup> and an electron tail population produced by electron cyclotron heating<sup>55</sup> have all driven Alfvén eigenmodes unstable. Instability is observed in essentially all toroidal confinement configurations: tokamaks,<sup>52,53</sup>

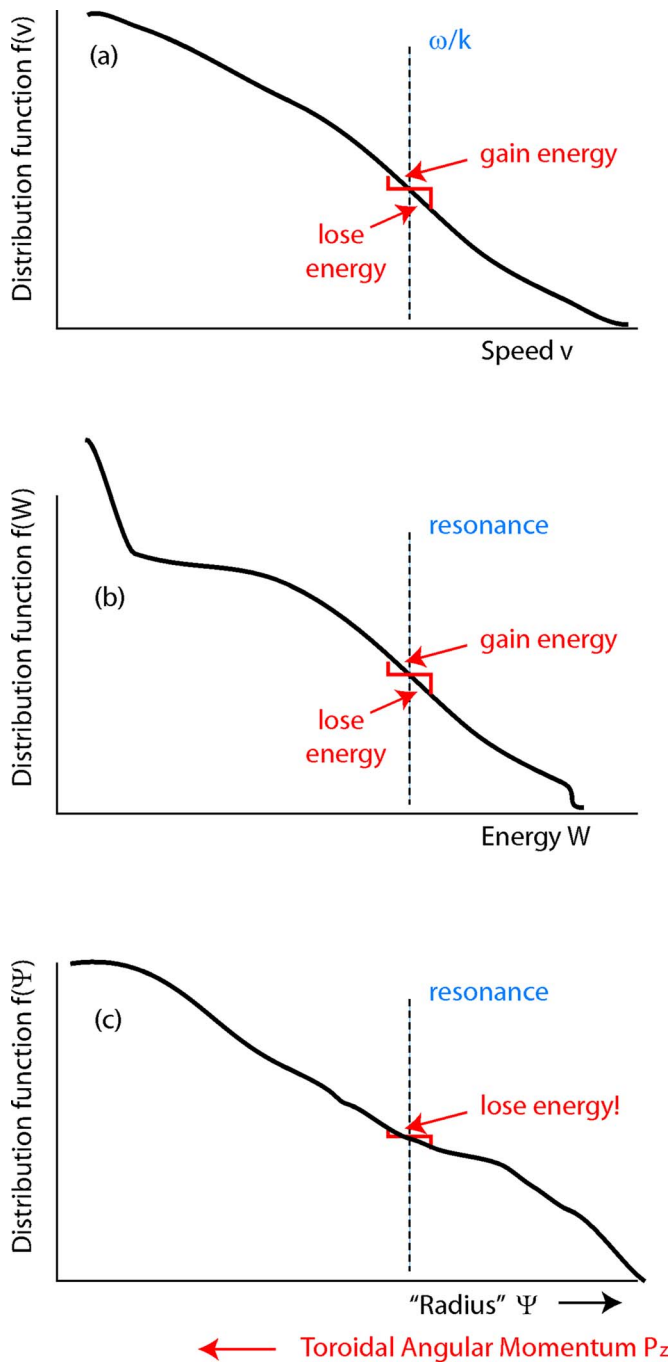


FIG. 12. (Color online) Illustration of the dependence of EP drive (or damping) on the slope of the distribution function. (a) Classic Landau damping situation: for a monotonically decreasing distribution function there are more particles that gain energy from the wave than lose energy, so the wave damps. (b) The energy distribution typically is monotonically decreasing, so the wave damps. (c) The distribution function is usually peaked on axis. The toroidal angular momentum  $P_z$  has the opposite dependence on radius than the flux function, so a peaked distribution function has a positive gradient  $\partial f/\partial P_z$  and gives net energy to the wave.

stellarators,<sup>34</sup> spherical tokamaks,<sup>56</sup> and a reversed field pinch (even without an EP population).<sup>57</sup>

Several factors determine the actual energy exchange. First, the relative strength of the various resonances depends on the amplitudes of the poloidal harmonics that make up the eigenmode and on the Fourier amplitudes of the drift velocity. Second, as in Landau damping [Fig. 12(a)], the net en-

ergy exchange between the particles and the wave depends on the slope of the distribution function. Particles with speed slightly below the resonant velocity gain energy, while particles with speeds slightly above the resonant velocity lose energy. If the distribution function is monotonically decreasing along a coordinate that defines the resonance, the particles damp the wave. Most EP distribution functions monotonically decrease with increasing energy ( $\partial f/\partial W < 0$ ), so the energy distribution usually damps the wave [Fig. 12(b)]. (This is true both for the slowing-down distributions that commonly occur for fusion products and neutral-beam injection and for the Boltzmann distribution that often occurs during wave heating.) Wave growth is usually driven by the free energy in the spatial gradient. The canonical toroidal angular momentum is

$$P_z = mRv_z - Ze\Psi, \quad (9)$$

where  $m$  and  $Ze$  are the ion mass and charge and  $\Psi = RA_z$  is the poloidal flux. ( $A_z$  is the toroidal component of the magnetic vector potential.) Note that  $P_z$  decreases when  $\Psi$  increases. An EP profile that peaks on axis has  $\partial f/\partial \Psi < 0$  but  $\partial f/\partial P_z > 0$  [Fig. 12(c)]. The wave gains energy at the expense of the particles. The energy transfer is proportional to

$$\gamma \propto \omega \frac{\partial f}{\partial W} + n \frac{\partial f}{\partial P_z}. \quad (10)$$

(Since the magnetic moment  $\mu$  is not altered by low-frequency Alfvén waves,  $\partial f/\partial \mu$  is irrelevant to the energy transfer.) Alfvén eigenmodes with  $n \neq 0$  break the toroidal symmetry of the plasma. If the ions are fast, the toroidal frequency  $\omega_z$  is large and the resonance condition [Eq. (8)] is satisfied for a significant fraction of the population; if, in addition, the spatial gradient of the resonant particles is large, the energetic particles can strongly drive the mode.

The strongest confirmation of these ideas was obtained in the TFTR D-T experiments. Alpha-particle driven TAEs were not ordinarily observed. Calculations indicated that the large beam-ion population was strongly damping the TAEs through the  $\partial f/\partial W$  term. Based on these calculations, theorists predicted<sup>58,59</sup> that, if beam-ion Landau damping could be suppressed, the spatial gradient of the alpha particles would destabilize TAEs and suggested<sup>59</sup> that this condition could be achieved after neutral-beam injection, since the beam-ion pressure would decay much faster than the alpha pressure. Indeed, when the experiment was conducted, alpha-driven TAEs were observed  $\sim 150$  ms after beam injection,<sup>60</sup> as theoretically predicted.

The third factor governing energy exchange is the alignment of the orbit with the eigenmode. Because the toroidal symmetry is more strongly broken for higher toroidal mode numbers, the extracted energy scales linearly with  $n$  as long as the orbit is small compared to the radial extent of the mode. However, if the orbit exceeds the radial extent of the mode, the efficiency of energy transfer declines. Since the radial extent shrinks approximately as  $n^{-1}$ , there is generally a particular mode number  $n$  that maximizes the fast-ion drive. Theoretically, the drive is largest when the orbit size approximately matches the eigenmode spatial extent.<sup>61</sup> Ex-

perimentally, the most unstable toroidal mode numbers of TAEs in tokamaks approximately follow  $k_\theta \rho_{EP} \approx 1$  scaling.<sup>12,62</sup> (Here  $k_\theta$  is the poloidal wave vector of the mode and  $\rho_{EP}$  is the energetic particle gyroradius.)

In practice, these various factors are far too complicated to calculate analytically, so the wave-particle energy transfer is computed numerically. An accurate quantitative measurement of the EP drive  $\gamma_L$  has not been obtained yet.

Instability occurs when the EP drive overcomes the intrinsic damping of the background plasma  $\gamma_d$ . Theoretically, important damping mechanisms include ion Landau damping,<sup>22</sup> collisional damping by trapped electrons,<sup>63</sup> continuum damping by the portion of the eigenfunction that extends spatially into the continuum,<sup>64,65</sup> and “radiative” damping,<sup>66</sup> which is a kind of tunneling in frequency to modes in the continuum. Experimentally, the most accurate technique for inferring damping rates is to sweep the frequency of an antenna across a resonance to measure the quality factor  $Q$  (Fig. 7). In both theory and experiment, the damping rates are very sensitive to plasma parameters such as the  $q$  profile. Presently, it is unclear whether observed damping rates are explicable by existing theory.<sup>67</sup>

#### IV. ENERGETIC PARTICLE MODES

The Alfvén modes discussed so far are normal modes of the background plasma. Even in the absence of energetic particles, these modes are weakly damped waves that can be excited, for example, by an external antenna (Fig. 7). Energy extracted from the energetic particles overcomes the intrinsic damping of the medium and drives the wave unstable but does not alter its basic properties. The EP density is low,  $n_{EP} \ll n_e$ , so the energetic particles do not determine the basic dielectric properties of the medium. In mathematical terms, the energetic particles affect the imaginary part of the wave frequency  $\omega$  but not the real part.

A new class of instabilities, the energetic particle modes (EPM),<sup>68</sup> appear when the EP pressure is comparable to the pressure of the thermal plasma. The mode structure often resembles the eigenfunction of a related gap mode but the EPM constitutes a separate wave branch with a distinctive dispersion relation. Both the frequency and growth rate (real and imaginary parts of  $\omega$ ) depend sensitively on the EP distribution function, with the frequency usually corresponding to a characteristic frequency of the EP orbital motion. If the drive is strong enough, an EPM may be unstable despite having a frequency in the Alfvén continuum. For example, concurrent publications by three different theoretical groups<sup>69–71</sup> found a mode called the resonant-TAE that has a polarization and mode structure similar to the TAE but a frequency that changes when the EP distribution function is changed. Essentially, an EPM is a type of beam mode with the background plasma supplying neutralizing charge.

Experimentally, instabilities in the Alfvén continuum are often observed during intense neutral-beam injection. Semi-periodic bursts of EPM activity are common. Within each burst, the mode frequency rapidly changes as the EP distribution function is altered by the instability. (Note, however, that normal modes of the background plasma can also exhibit

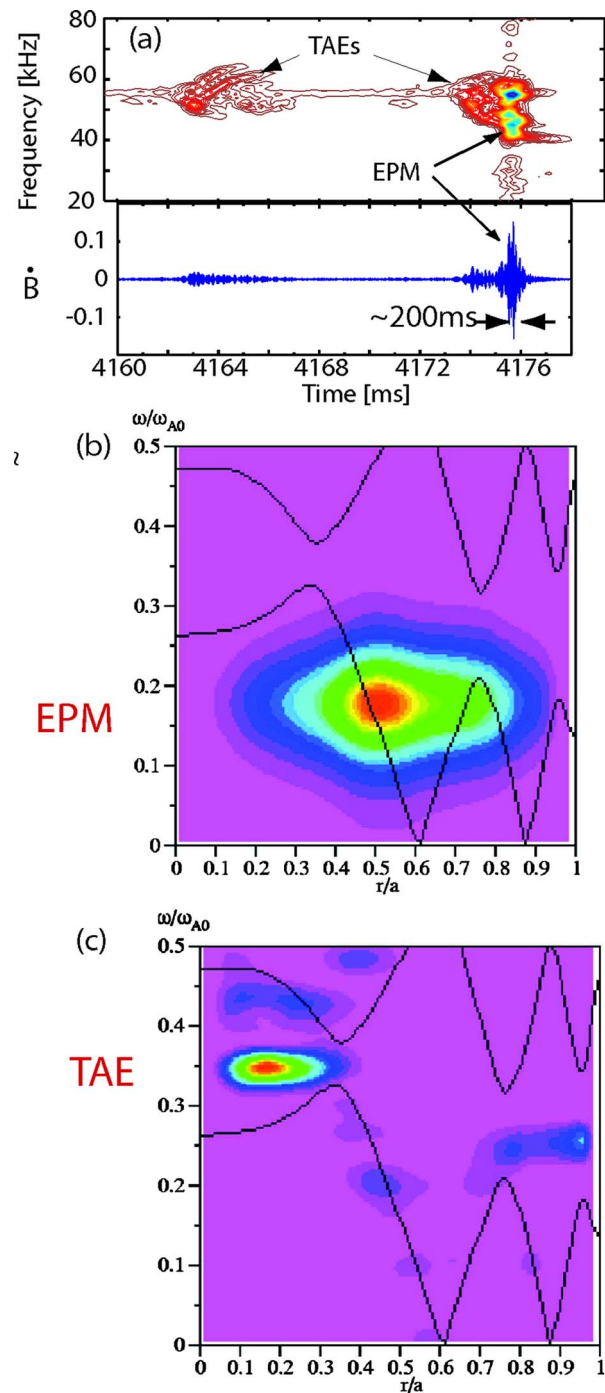


FIG. 13. (Color online) (a) Experimental magnetics data from the JT-60U tokamak during beam injection showing bursts of Alfvén activity. Modeling shows that the smaller amplitude bursts are (c) TAEs with frequencies in the gap of the Alfvén continuum but the large amplitude modes with rapid frequency chirping are (b) EPMs with frequencies that can lie in the continuum. [In the original experimental papers, the TAEs were called “fast frequency-sweeping” modes and the EPMs were called “abrupt large-amplitude events (ALE).”] Adapted from Refs. 73 and 74.

rapid frequency chirping, see Sec. V A.) The first rapidly chirping instabilities in the TAE frequency band were observed on DIII-D.<sup>72</sup> During intense neutral-beam injection into JT-60U, both normal modes and EPMs are observed [Fig. 13(a)].<sup>73</sup> Theoretical analysis of these data with a code that treats the EPs kinetically and uses MHD to model the

background plasma shows that the large amplitude mode with the large frequency sweep is an EPM with a frequency that can overlap the continuum, while the smaller amplitude modes with weaker frequency chirping are TAEs [Figs. 13(b) and 13(c)].<sup>74</sup>

## V. NONLINEAR DYNAMICS

Once instability occurs, the mode amplitude grows until changes in the EP distribution reduce the EP drive or until the damping increases through, for example, coupling to stable waves. Saturation at a steady level and repetitive bursts of activity are both commonly observed.

### A. Berk–Breizman model

A relatively simple model developed by Berk, Breizman (BB), and co-workers has been surprisingly successful in explaining the complex phenomenology observed in experiments. They explore a simplified system: the classic “bump-on-tail” Bernstein–Greene–Kruskal (BGK) (Ref. 75) problem of a distribution function that excites electrostatic waves. The basic insight is that the  $P_\zeta$  gradient that drives EP instabilities is analogous to the velocity-space gradient that drives the instability in the BGK problem (Fig. 12). Berk *et al.* found that, independent of the particular physical system, four characteristic frequencies determine the nonlinear dynamics of the resonant particles.<sup>76,77</sup> Instability occurs when the linear growth rate  $\gamma_L$  of the kinetic drive exceeds the damping of the background plasma  $\gamma_d$ . The subsequent evolution depends on the characteristic bounce frequency of the resonant particles that are trapped in the finite amplitude wave  $\omega_b$  compared to the rate  $\nu_{\text{eff}}$  that particles leave and enter the resonance region in phase space due to collisions (or other stochastic processes). In their model,<sup>78</sup> frequency chirping is associated with the formation of holes and clumps in the phase space that describes the EP distribution function. When collisions are weak, these phase-space structures persist and frequency chirping is possible. When the effective collision rate is large, the structures are rapidly destroyed and no frequency chirping occurs.<sup>79</sup> In the weakest collisional regime, the Berk–Breizman hole-clump model applies to a single normal mode. An explosive precursor occurs<sup>77</sup> that evolves into the formation of a hole and clump in phase space;<sup>80</sup> the wave frequency locks onto the linear resonance frequency of the resonant particles. Next, the dissipation that is present in the background plasma forces the wave-trapped resonant particles to move in phase space in such a way that the excited waves release energy while still nearly maintaining the wave amplitude. For the bump-on-tail problem and the Alfvén wave problem, this causes an increase of the hole resonant frequency while causing a decrease of the clump resonant frequency. With various weak perturbation assumptions, including that the gradient of the equilibrium phase-space distribution does not change appreciably as the phase-space structures move in phase space, the Berk–Breizman hole-clump model predicts that the frequency chirp  $\delta\omega$  tracks the phase-space perturbation, with a time evolution

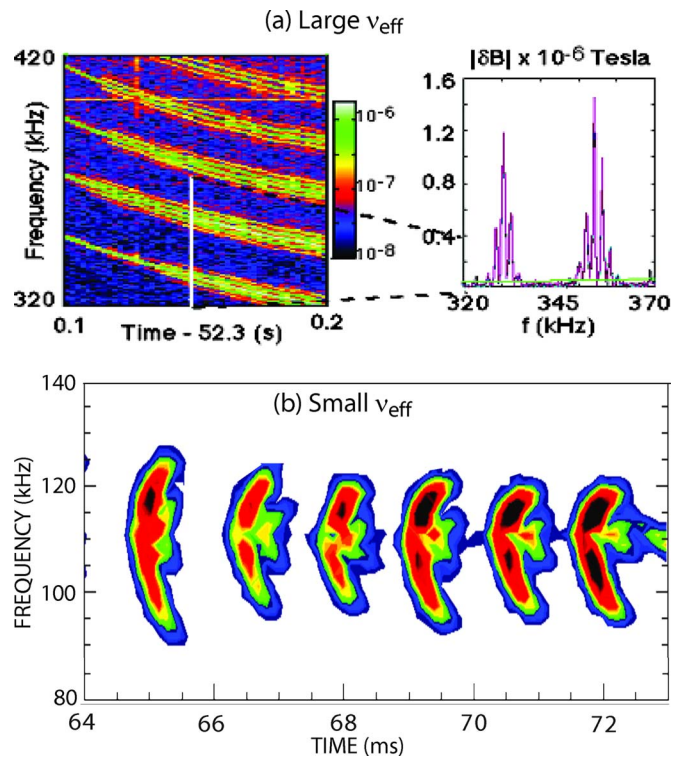


FIG. 14. (Color online) Examples of two phenomena that are successfully explained by the Berk–Breizman model. (a) In the JET tokamak, modes that are driven unstable by rf-accelerated tail ions undergo frequency splitting. This behavior is predicted when the resonant particles are scattered quickly out of resonance (large  $\nu_{\text{eff}}$ ). Adapted from Ref. 85. (b) In the MAST spherical tokamak, modes that are driven unstable by neutral beam ions begin at the TAE frequency, then chirp upward and downward in frequency. This behavior is predicted for waves with low values of  $\nu_{\text{eff}}$ . From Ref. 87.

$$\delta\omega \propto \sqrt{\delta t}. \quad (11)$$

For stronger drive,  $\delta f \propto t$  is predicted.<sup>81</sup>

Many features of the BB model are qualitatively consistent with experimental observations. A semiempirical predator-prey model where the mode amplitude “preys” on the fast-ion population accounts for many features of the cycle of instability bursts and particle losses that are often observed;<sup>82</sup> the possibility of repetitive burst cycles is a natural consequence of the BB model when beam fueling is included.<sup>83</sup> TFTR observations of the saturated amplitude near the linear stability threshold, of multiple modes well above threshold, of predator-prey burst cycles during neutral-beam injection, and of changes in mode amplitude when the ion cyclotron heating power is turned off can all be explained in terms of changes in  $\gamma_L$ ,  $\gamma_d$ ,  $\omega_b$ , and  $\nu_{\text{eff}}$ .<sup>3,84</sup> Observations on JET that a single-frequency mode can split into multiple lines [Fig. 14(a)]<sup>85</sup> or even become chaotic<sup>86</sup> as the fast-ion drive increases are consistent with the BB model. The time evolution of a frequency chirping TAE mode [Fig. 14(b)] in the mega-ampere spherical tokamak (MAST) agrees well with modeling based on BB theory in agreement with Eq. (11),<sup>87</sup> also, the repetitive cycle of chirping bursts is reproduced by the model.<sup>88</sup> Modes in MAST that chirp upward in frequency, downward, or both directions can also be explained.<sup>89</sup>

## B. Fast-ion transport

Theoretically, the energy delivered by a particle to the wave is related to changes in its constants of motion. Since the mode frequency is much smaller than the cyclotron frequency, the magnetic moment is conserved,  $\Delta\mu=0$ . Thus, the perpendicular energy  $W_{\perp}$  decreases if the particle moves outward in major radius to a region of lower magnetic field. For interaction with a single toroidal mode, the change in energy is related to the change in toroidal angular momentum by the simple relationship<sup>90</sup>

$$\Delta P_{\zeta} = (n/\omega)\Delta W. \quad (12)$$

In the normal situation, particles that lose energy move from the center of the plasma outward in the minor radius. Typically, for low-frequency Alfvén modes, the relative change in toroidal angular momentum is much larger than the relative change in energy,  $\Delta W/W = O(0.1\Delta P_{\zeta}/P_{\zeta})$ .

Four types of irreversible transport are distinguished (Fig. 10): phase-locked convective, topological change in orbit, diffusive transport, and avalanches. Phase-locked convective transport can occur for a single global mode if the resonant particles stay in phase with the wave as they steadily march out of the machine.<sup>91</sup> The resultant transport scales linearly with mode amplitude. Transport of this type often occurs for EPs, as the frequency of the wave readily adjusts to match the changing orbital frequencies of the particles as they move radially, thus preserving resonance. A simulation of the ‘‘ALE’’ EPM shows transport of this sort and agrees reasonably well with experimental observations.<sup>74</sup> Measurements of beam-ion transport in early DIII-D experiments also were consistent with this mechanism.<sup>1</sup> This type of loss is the likely explanation for the damage to optical components near the midplane mentioned in the Introduction. Convective losses of this sort often scale linearly with mode amplitude  $\tilde{B}$ .

When a particle changes its constants of motion in response to the wave, its orbit may cross a topological boundary. Because the displacement from flux surfaces is large for EPs, the effective step length of such a change can be quite large. The most extreme example is a transition onto a loss orbit. Transport of this type is often observed on scintillator probes at the plasma edge: the mode causes an enhanced signal at the same pitch angle that ordinary prompt losses occur.<sup>92</sup> Oscillations in the loss signal at the TAE frequency were recently observed.<sup>93</sup> Transport of fast ions onto loss orbits caused by magnetic ripple in the toroidal field probably caused the TFTR vacuum accident mentioned in the Introduction.<sup>2</sup>

For gap modes of modest spatial extent, diffusive transport is theoretically expected to predominate.<sup>94</sup> Particles receive many  $\mathbf{E} \times \mathbf{B}$  kicks from the wave that are decorrelated. Island overlap in regions of phase space may enhance the stochastic transport. The resultant transport is expected to scale as the mode amplitude squared,  $\tilde{B}^2$ . In recent experiments on the Compact Helical System (CHS) stellarator, both convective and diffusive transport were observed with the expected linear and quadratic scalings with mode amplitude.<sup>95</sup>

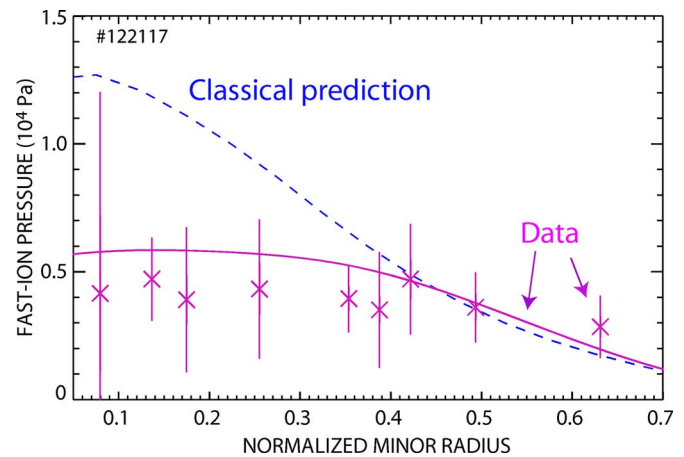


FIG. 15. (Color online) The radial fast-ion profile measured during Alfvén activity in the DIII-D tokamak is much flatter than classically predicted (dashed line). The data are from equilibrium reconstructions (solid line) and fast-ion D-alpha measurements (symbols). Adapted from Ref. 101.

The fourth type of transport occurs when transport of EPs from one position steepens the spatial gradient at a new position, destabilizing a mode there.<sup>96</sup> The process is analogous to an avalanche of a sandpile or the collapse of dominos. A propagating wavefront of this type is observed in simulations.<sup>97</sup> A threshold in mode amplitude to initiate an avalanche is expected. Experimentally, a clear example of phenomena is expected. Experimentally, a clear example of phenomena is observed in the National Spherical Torus Experiment (NSTX) during beam injection. When the TAE amplitude is small, only a few toroidal mode numbers are excited and the fast-ion transport is small. When the TAE amplitude grows larger, many toroidal modes are excited and significant fast-ion transport is measured.<sup>32</sup>

Although a qualitative understanding of EP transport is well established, quantitative agreement between theory and experiment is currently lacking. To obtain agreement with observed fast-ion transport in tokamak neutral-beam injection experiments with super-Alfvénic fast ions and TAE activity, the wave amplitudes in the simulations needed to be an order of magnitude larger than the measured values.<sup>98,99</sup> In recent work during neutral-beam injection in reversed-shear plasmas, local fluctuation diagnostics accurately measured the electron temperature and density fluctuations; the observed RSAE and TAE mode structures (Fig. 6) agree well with MHD theory.<sup>28,100</sup> Multiple diagnostics measured strong flattening of the fast-ion profile in the same discharge (Fig. 15). However, when an orbit-following code computes the expected fast-ion transport in the measured wave fields, much less transport is predicted than is observed experimentally.<sup>101</sup>

## VI. THE FRONTIER

Previous sections summarize the current state of knowledge for EP instabilities. The basic properties of Alfvén gap modes and EP orbits explained there are accepted by virtually all specialists in the field. In contrast to previous sections, this section focuses on gaps in our knowledge and

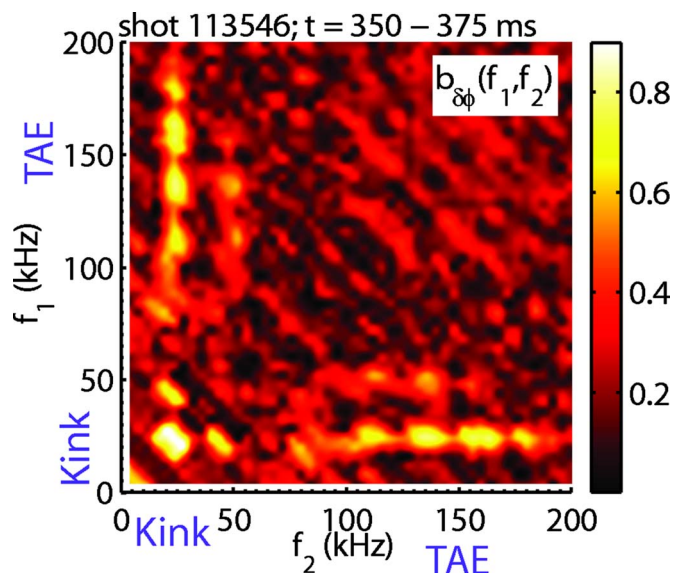


FIG. 16. (Color online) Bicoherence of a reflectometer signal during beam injection into the NSTX spherical tokamak. The analysis indicates that TAE waves with frequencies between 100–200 kHz interact nonlinearly with a low-frequency ( $\sim 20$  kHz) mode. Adapted from Ref. 107.

identifies future research opportunities. Here, the discussion is necessarily more subjective and controversial.

Two important gaps in knowledge were already mentioned in previous sections. The first of these is accurate prediction of the intrinsic mode damping by the background plasma. A gyrokinetic code called PENN<sup>102</sup> has successfully predicted the magnitude and parametric dependencies of a number of JET wave damping measurements of toroidal modes with  $n=1$  and 2<sup>103,104</sup> but the results are viewed skeptically by the theoretical community.<sup>67</sup> An intense experimental effort is currently underway worldwide<sup>105,106</sup> to use antenna excitation experiments to measure the damping rates of modes with higher toroidal mode numbers than in the original JET experiments.

The second major gap identified in previous sections is the successful quantitative prediction of fast-ion transport. Since the Lorentz force law is surely correct, something must be lacking in our representation of the wave fields or perhaps the modes that actually cause the spatial transport are not the Alfvén gap modes that seem to dominate the spectrum. In addition to new experiments, many new fluctuation and fast-ion diagnostics are being installed worldwide to address this important issue.

Generally speaking, the field is currently transitioning from an emphasis on linear mode identification to an emphasis on understanding and predicting the nonlinear dynamics of unstable modes. As this transition occurs, measurements that pinpoint the nonlinear interactions will increase in importance. Techniques that are commonplace in the study of thermal transport will find increasing application in EP physics. A recent example is bicoherence analysis of EP instabilities in NSTX, where strong coupling between Alfvén instabilities and lower-frequency MHD was observed (Fig. 16).<sup>107</sup>

The most advanced simulation codes have been based on “hybrid” models that treat the energetic particles kinetically

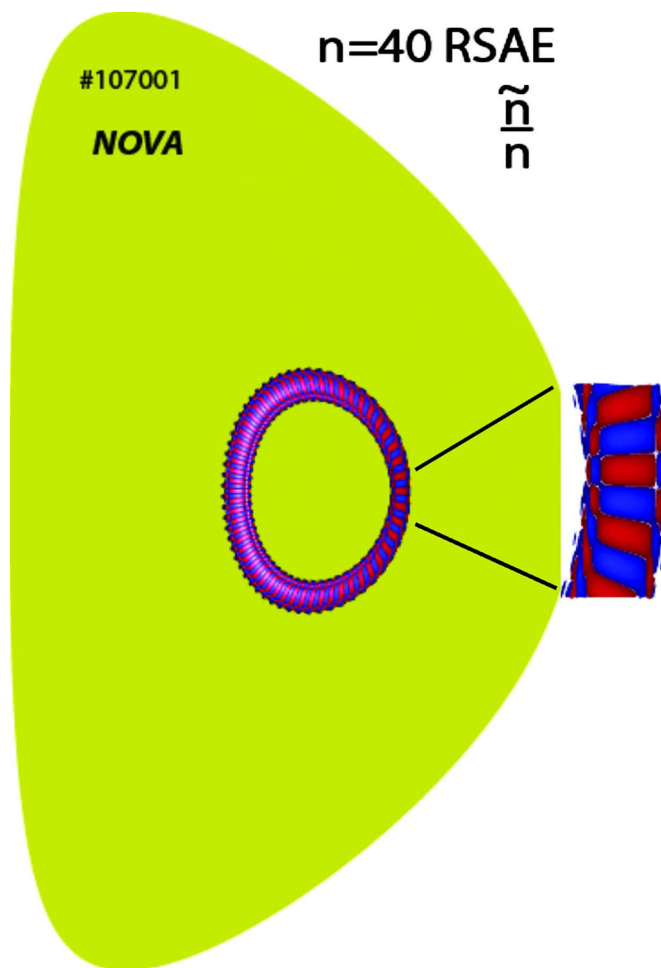


FIG. 17. (Color online) Calculated mode structure that is consistent with experimental data during beam injection into the DIII-D tokamak. Very high toroidal mode numbers with a spatial scale that approaches the gyroradius of thermal ions are inferred. Adapted from Refs. 108 and 120.

but use MHD to describe the background plasma. A number of recent observations suggest that, for at least some phenomena, a more sophisticated treatment of the thermal plasma is required.

- In the presence of a large ion temperature gradient, instabilities with toroidal mode numbers up to  $n \leq 40$  are inferred in DIII-D (Fig. 17).<sup>108</sup> Calculations suggest that the highest  $n$  modes are driven by the thermal ion population.
- Detailed comparison of electron temperature fluctuations with electron density fluctuations suggests that, in some cases, MHD closure does not properly describe the relationship between  $\tilde{T}_e$  and  $\tilde{n}_e$ .<sup>109</sup>
- New EP-driven modes in a low-frequency band are observed that seem to be caused by coupling of Alfvén waves with acoustic waves.<sup>47</sup> The proper treatment of parallel electric fields in stability analysis of these modes require a kinetic description of the thermal plasma.

In addition, it is likely that accurate predictions of background damping require a gyrokinetic treatment<sup>67</sup> and it is possible that the additional wave fields needed to explain fast-ion transport are associated with modification of the wave polarization by kinetic effects.

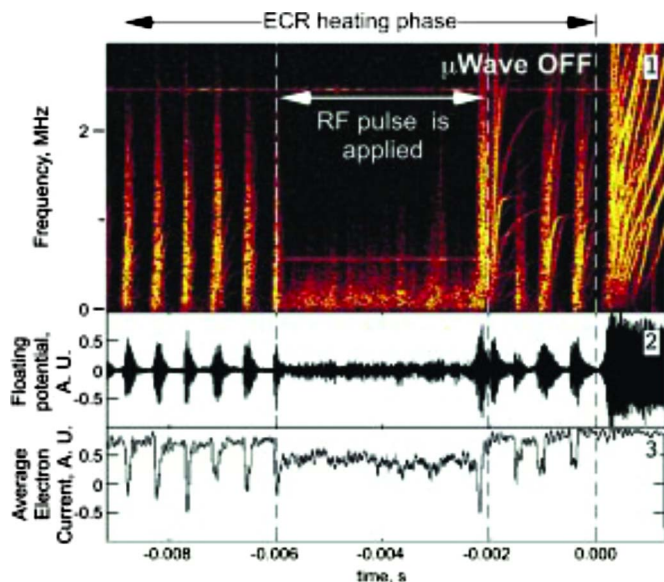


FIG. 18. (Color online) Example of control of an EP-driven instability. (This instability is an interchange mode, not an Alfvén wave.) Energetic electrons in a dipole experiment drive the instability and cause frequency sweeping that is consistent with the Berk–Breizman model. The application of 50 W of rf power that increases the effective collisionality  $\nu_{\text{eff}}$  of the wave-trapped electrons alters the nonlinear dynamics, replacing the large bursts with relatively steady noise. Reused with permission from Ref. 114. Copyright © 2003 American Institute of Physics.

Obviously, the ITER project is a major frontier for EP physics. There are many important differences between ITER and existing devices in regard to EP-driven instabilities.<sup>110</sup> First, the EP distribution function is anisotropic in current experiments but the alpha-particle distribution function from D-T reactions is nearly isotropic. Second, in current experiments, the intrinsic damping of the modes seems to depend sensitively on mode coupling to other heavily damped waves (“radiative damping”). The magnitude of this coupling is predicted to depend on the normalized thermal gyroradius, which is much smaller in ITER. Third, in a reactor, both the radial extent of the instabilities and the fast-ion orbit contract relative to current experiments, so the fast-ion transport will change. Fourth, when instability occurs, a larger number of modes are likely to be unstable, so the mechanism of nonlinear saturation may shift from fast-ion transport to mode-mode coupling.

Beyond ITER, the challenge for the field is to control EP-driven instabilities and possibly even exploit them for beneficial purposes. Fisch and co-workers noted that in an ideal reactor alpha particles would transfer their energy directly to fuel ions rather than transferring their energy to the lossy electron population.<sup>111</sup> Alfvén gap modes could play a role in this but an additional wave is needed to extract the energy efficiently.<sup>111</sup> Although energy channeling remains a distant dream, beneficial effects of Alfvén instabilities already occur in some experiments. For example, in DIII-D, redistribution of injected beam ions can help sustain an off-axis current that allows access to a higher confinement regime. In a set of discharges with weak, moderate, and strong Alfvén activity, the discharge with the most favorable current evolution to obtain the desired current profile had moderate

EP-driven instabilities.<sup>50,112</sup> Exploitation of Alfvén instabilities will require precise, efficient control tools. To that end, in a recent experiment, local application of electron cyclotron heating near the minimum of the  $q$  profile suppressed RSAE activity while scarcely affecting the unstable TAEs.<sup>113</sup> The fast-ion transport was reduced when the RSAEs were suppressed. In principle, one can imagine using such a tool to modify the fusion-product profile in a reactor. Another possibility is to alter the nonlinear dynamics of unstable modes. The clearest demonstration to date of this possibility is for an interchange instability that is driven by energetic electrons,<sup>114</sup> rather than for an Alfvén instability. In this experiment, local application of electron cyclotron heating altered the effective collisionality of electrons that were in resonance with the wave and suppressed rapid frequency chirping. The activity shifted from strong bursting of predator-prey type to a quasistaturated state at lower amplitude (Fig. 18). In a reactor, one can imagine using a similar technique to replace potentially catastrophic bursts with benign local flattening of the EP distribution function.

## ACKNOWLEDGMENTS

Helpful discussions with Sergei Sharapov, Simon Pinches, Boris Breizman, Nikolai Gorelenkov and, especially, Liu Chen, are gratefully acknowledged. D. Brower, N. Crocker, D. Darrow, A. Fasoli, E. Fredrickson, M. García-Muñoz, G. Kramer, M. Mauel, R. Nazikian, S. Pinches, S. Sharapov, K. Shinohara, J. Snipes, D. Spong, K. Toi, M. Van Zeeland, G. Vlad, A. Weller, R. White, R. Vann, S. Vincena, Y. Zhang, and S. Zweben contributed figures. The DIII-D group made many helpful suggestions.

This work was supported by the U.S. DOE.

- <sup>1</sup>H. H. Duong, W. W. Heidbrink, E. J. Strait, T. W. Petrie, R. Lee, R. A. Moyer, and J. G. Watkins, *Nucl. Fusion* **33**, 749 (1993).
- <sup>2</sup>R. B. White, E. Fredrickson, D. Darrow, M. Zarnstorff, R. Wilson, S. Zweben, K. Hill, Y. Chen, and G. Fu, *Phys. Plasmas* **2**, 2871 (1995).
- <sup>3</sup>K.-L. Wong, *Plasma Phys. Controlled Fusion* **41**, R1 (1999).
- <sup>4</sup>G. Vlad, F. Zonca, and S. Briguglio, *Riv. Nuovo Cimento* **22**, 1 (1999).
- <sup>5</sup>F. Zonca, S. Briguglio, L. Chen, G. Fogaccia, T. S. Hahm, A. V. Milovanov, and G. Vlad, *Plasma Phys. Controlled Fusion* **48**, B15 (2006).
- <sup>6</sup>B. Breizman, *AIP Conf. Proc.* **871**, 15 (2006).
- <sup>7</sup>L. Chen and F. Zonca, *Nucl. Fusion* **47**, S727 (2007).
- <sup>8</sup>W. W. Heidbrink and G. J. Sadler, *Nucl. Fusion* **34**, 535 (1994).
- <sup>9</sup>S. D. Pinches, H. L. Berk, D. N. Borba *et al.*, *Plasma Phys. Controlled Fusion* **46**, B187 (2004).
- <sup>10</sup>ITER Physics Expert Group on Energetic Particles, Heating, and Current Drive and ITER Physics Basis Editors, *Nucl. Fusion* **39**, 2471 (1999).
- <sup>11</sup>A. Fasoli, C. Gormenzano, H. L. Berk *et al.*, *Nucl. Fusion* **47**, S264 (2007).
- <sup>12</sup>W. W. Heidbrink, *Phys. Plasmas* **9**, 2113 (2002).
- <sup>13</sup>S. D. Pinches, “Nonlinear interaction of fast particles with Alfvén waves in tokamaks,” Ph.D. thesis, University of Nottingham, 1996, <http://www.rzg.mpg.de/~sip/thesis/node1.html>.
- <sup>14</sup>R. B. White, *The Theory of Toroidally Confined Plasmas*, 2nd ed. (Imperial College Press, London, 2001).
- <sup>15</sup>W. Gekelman, S. Vincena, and D. Leneman, *Plasma Phys. Controlled Fusion* **39**, 101 (1997).
- <sup>16</sup>J. W. Strutt, *Philos. Mag.* **24**, 145 (1887).
- <sup>17</sup>Y. Zhang, W. W. Heidbrink, H. Boehmer *et al.*, *Phys. Plasmas* **15**, 012103 (2008).
- <sup>18</sup>D. A. D’Ippolito and J. P. Goedbloed, *Plasma Phys.* **22**, 1091 (1980).
- <sup>19</sup>G. Y. Fu and J. W. Van Dam, *Phys. Fluids B* **1**, 1949 (1989).
- <sup>20</sup>M. S. Chu, J. M. Greene, L. L. Lao, A. D. Turnbull, and M. S. Chance, *Phys. Fluids B* **4**, 3713 (1992).

- <sup>21</sup>R. L. Dewar, R. C. Grimm, J. L. Johnson, E. A. Frieman, J. M. Greene, and P. H. Rutherford, *Phys. Fluids* **17**, 930 (1974).
- <sup>22</sup>R. Betti and J. P. Freidberg, *Phys. Fluids B* **4**, 1465 (1992).
- <sup>23</sup>N. Nakajima, C. Z. Cheng, and M. Okamoto, *Phys. Fluids B* **4**, 1115 (1992).
- <sup>24</sup>Y. I. Kolesnichenko, V. V. Lutsenko, H. Wobig, Y. V. Yakovenko, and O. P. Fesenyuk, *Phys. Plasmas* **8**, 491 (2001).
- <sup>25</sup>D. A. Spong, R. Sanchez, and A. Weller, *Phys. Plasmas* **10**, 3217 (2003).
- <sup>26</sup>E. Yablonovitch, T. J. Gmitter, R. D. Meade, A. M. Rappe, K. D. Brommer, and J. D. Joannopoulos, *Phys. Rev. Lett.* **67**, 3380 (1991).
- <sup>27</sup>B. N. Breizman, M. S. Pekker, and S. E. Sharapov, *Phys. Plasmas* **12**, 112506 (2005).
- <sup>28</sup>M. A. Van Zeeland, G. J. Kramer, M. E. Austin, R. L. Boivin, W. W. Heidbrink, M. A. Makowski, G. R. McKee, R. Nazikian, W. W. Solomon, and G. Wang, *Phys. Rev. Lett.* **97**, 135001 (2006).
- <sup>29</sup>S. E. Sharapov, B. Alper, H. L. Berk *et al.*, *Phys. Plasmas* **9**, 2027 (2002).
- <sup>30</sup>C. Z. Cheng, L. Chen, and M. Chance, *Ann. Phys.* **161**, 21 (1985).
- <sup>31</sup>C. Z. Cheng and M. S. Chance, *Phys. Fluids* **29**, 3695 (1986).
- <sup>32</sup>E. D. Fredrickson, R. E. Bell, D. S. Darrow *et al.*, *Phys. Plasmas* **13**, 056109 (2006).
- <sup>33</sup>A. Fasoli, D. Borba, C. Gormezano *et al.*, *Plasma Phys. Controlled Fusion* **39**, B287 (1997).
- <sup>34</sup>A. Weller, D. A. Spong, R. Jaenicke, A. Lazaros, F. P. Penningsfeld, and S. Sattler, *Phys. Rev. Lett.* **72**, 1220 (1994).
- <sup>35</sup>A. Weller, M. Anton, J. Geiger, M. Hirsch, R. Jaenicke, A. Werner, C. Nührenberg, and E. Sallander, *Phys. Plasmas* **8**, 931 (2001).
- <sup>36</sup>A. D. Turnbull, E. J. Strait, W. W. Heidbrink, M. S. Chu, H. H. Duong, J. M. Greene, L. L. Lao, T. S. Taylor, and S. J. Thompson, *Phys. Fluids B* **5**, 2546 (1993).
- <sup>37</sup>A. Fasoli, J. B. Lister, S. Sharapov *et al.*, *Nucl. Fusion* **35**, 1485 (1995).
- <sup>38</sup>G. J. Kramer, M. Saigusa, T. Ozeki, Y. Kusama, H. Kimura, T. Oikawa, K. Tobita, G. Y. Fu, and C. Z. Cheng, *Phys. Rev. Lett.* **80**, 2594 (1998).
- <sup>39</sup>K. Toi, S. Ohdachi, S. Yamamoto *et al.*, *Nucl. Fusion* **44**, 217 (2004).
- <sup>40</sup>W. W. Heidbrink, E. J. Strait, M. S. Chu, and M. S. Turnbull, *Phys. Rev. Lett.* **71**, 855 (1993).
- <sup>41</sup>K. Appert, R. Gruber, F. Troyon, and J. Vaclavik, *Plasma Phys.* **24**, 1147 (1982).
- <sup>42</sup>N. N. Gorelenkov, E. Fredrickson, E. Belova, C. Z. Cheng, D. Gates, S. Kaye, and R. White, *Nucl. Fusion* **43**, 228 (2003).
- <sup>43</sup>G. Y. Fu, *Phys. Plasmas* **2**, 1029 (1995).
- <sup>44</sup>R. Nazikian, G. Y. Fu, S. H. Batha *et al.*, *Phys. Rev. Lett.* **78**, 2976 (1997).
- <sup>45</sup>A. Fasoli, J. B. Lister, S. Sharapov *et al.*, *Phys. Rev. Lett.* **76**, 1067 (1996).
- <sup>46</sup>E. D. Fredrickson, N. Gorelenkov, C. Z. Cheng *et al.*, *Phys. Rev. Lett.* **87**, 145001 (2001).
- <sup>47</sup>N. Gorelenkov, *Phys. Lett. A* **370/371**, 70 (2007).
- <sup>48</sup>S. J. Zweben, R. V. Budny, D. S. Darrow, S. S. Medley, R. Nazikian, B. C. Stratton, E. J. Synakowski, G. Taylor, and the TFTR Group, *Nucl. Fusion* **40**, 91 (2000).
- <sup>49</sup>Y. Todo and T. Sato, *Phys. Plasmas* **5**, 1321 (1998).
- <sup>50</sup>K. L. Wong, W. W. Heidbrink, E. Ruskov, C. C. Petty, C. M. Greenfield, R. Nazikian, and R. Budny, *Nucl. Fusion* **45**, 30 (2005). The ITER analysis in this paper makes the erroneous assumption that counter-circulating alphas will not resonate with TAEs.
- <sup>51</sup>S. D. Pinches, V. G. Kiptily, S. E. Sharapov *et al.*, *Nucl. Fusion* **46**, S904 (2006).
- <sup>52</sup>K. L. Wong, R. J. Fonck, S. F. Paul *et al.*, *Phys. Rev. Lett.* **66**, 1874 (1991).
- <sup>53</sup>W. W. Heidbrink, E. J. Strait, E. Doyle, G. Sager, and R. T. Snider, *Nucl. Fusion* **31**, 1635 (1991).
- <sup>54</sup>J. R. Wilson, M. G. Bell, H. Biglari *et al.*, "ICRF heating on TFTR-Effect on stability and performance," in *Plasma Physics and Controlled Nuclear Fusion Research 1992* (IAEA, Vienna, 1993), Vol. 1, p. 661.
- <sup>55</sup>D. Brower, private communication (2007).
- <sup>56</sup>K. G. McClements, M. P. Gryaznevich, S. E. Sharapov, R. J. Akers, L. C. Appel, G. F. Counsell, C. M. Roach, and R. Majeski, *Plasma Phys. Controlled Fusion* **41**, 661 (1999).
- <sup>57</sup>G. Regnoli, H. Bergsaker, E. Tennfors, and F. Zonca, *Phys. Plasmas* **12**, 042502 (2005).
- <sup>58</sup>D. A. Spong, C. L. Hedrick, and B. A. Carreras, *Nucl. Fusion* **35**, 1687 (1995).
- <sup>59</sup>G. Y. Fu, C. Z. Cheng, R. Budny, Z. Chang, D. S. Darrow, E. Fredrickson, E. Mazzucato, R. Nazikian, K. L. Wong, and S. Zweben, *Phys. Plasmas* **3**, 4036 (1996).
- <sup>60</sup>R. Nazikian, Z. Chang, E. D. Fredrickson *et al.*, *Phys. Plasmas* **3**, 593 (1996).
- <sup>61</sup>G. Y. Fu and C. Z. Cheng, *Phys. Fluids B* **4**, 3722 (1992).
- <sup>62</sup>W. W. Heidbrink, E. Fredrickson, N. N. Gorelenkov, A. W. Hyatt, G. Kramer, and Y. Luo, *Plasma Phys. Controlled Fusion* **45**, 983 (2003).
- <sup>63</sup>N. N. Gorelenkov and S. Sharapov, *Phys. Scr.* **45**, 163 (1992).
- <sup>64</sup>M. N. Rosenbluth, H. L. Berk, J. W. Van Dam, and D. M. Lindberg, *Phys. Rev. Lett.* **68**, 596 (1992).
- <sup>65</sup>F. Zonca and L. Chen, *Phys. Rev. Lett.* **68**, 592 (1992).
- <sup>66</sup>R. R. Mett and S. M. Mahajan, *Phys. Fluids B* **4**, 2885 (1992).
- <sup>67</sup>P. Lauber, S. Gunter, and S. D. Pinches, *Phys. Plasmas* **12**, 122501 (2005).
- <sup>68</sup>L. Chen, *Phys. Plasmas* **1**, 1519 (1994).
- <sup>69</sup>R. A. Santoro and L. Chen, *Phys. Plasmas* **3**, 2349 (1996).
- <sup>70</sup>C. Z. Cheng, N. N. Gorelenkov, and C. T. Hsu, *Nucl. Fusion* **35**, 1639 (1995).
- <sup>71</sup>S. Briguglio, C. Kar, F. Romanelli, G. Vlad, and F. Zonca, *Plasma Phys. Controlled Fusion* **37**, A279 (1995).
- <sup>72</sup>W. W. Heidbrink, *Plasma Phys. Controlled Fusion* **37**, 937 (1995).
- <sup>73</sup>K. Shinohara, Y. Kusama, M. Takechi *et al.*, *Nucl. Fusion* **41**, 603 (2001).
- <sup>74</sup>S. Briguglio, G. Fogaccia, G. Vlad, and F. Zonca, *Phys. Plasmas* **14**, 055904 (2007).
- <sup>75</sup>I. B. Bernstein, J. M. Greene, and M. D. Kruskal, *Phys. Rev.* **108**, 546 (1957).
- <sup>76</sup>H. L. Berk, B. N. Breizman, and H. Ye, *Phys. Rev. Lett.* **68**, 3563 (1992).
- <sup>77</sup>H. L. Berk, B. N. Breizman, and M. Pekker, *Phys. Rev. Lett.* **76**, 1256 (1996).
- <sup>78</sup>H. L. Berk, B. N. Breizman, J. Candy, M. Pekker, and N. V. Petviashvili, *Phys. Plasmas* **6**, 3102 (1999).
- <sup>79</sup>R. G. L. Vann, R. O. Dendy, G. Rowlands, T. D. Arber, and N. D'Ambrumenil, *Phys. Plasmas* **10**, 623 (2003).
- <sup>80</sup>H. L. Berk, B. N. Breizman, and N. V. Petviashvili, *Phys. Lett. A* **234**, 213 (1997); **238**, 408(E) (1998).
- <sup>81</sup>R. G. L. Vann, H. L. Berk, and A. R. Soto-Chavez, *Phys. Rev. Lett.* **99**, 025003 (2007).
- <sup>82</sup>W. W. Heidbrink, H. H. Duong, J. Manson, E. Wilfrid, C. Oberman, and E. J. Strait, *Phys. Fluids B* **5**, 2176 (1993).
- <sup>83</sup>H. L. Berk, B. N. Breizman, and M. Pekker, *Plasma Phys. Rep.* **23**, 778 (1997).
- <sup>84</sup>K. L. Wong, R. Majeski, M. Petrov, J. H. Rogers, G. Schilling, J. R. Wilson, H. L. Berk, B. N. Breizman, M. Pekker, and H. V. Wong, *Phys. Plasmas* **4**, 393 (1997).
- <sup>85</sup>A. Fasoli, B. N. Breizman, D. Borba, R. F. Heeter, M. S. Pekker, and S. E. Sharapov, *Phys. Rev. Lett.* **81**, 5564 (1998).
- <sup>86</sup>R. F. Heeter, A. F. Fasoli, and S. E. Sharapov, *Phys. Rev. Lett.* **85**, 3177 (2000).
- <sup>87</sup>S. D. Pinches, H. L. Berk, M. P. Gryaznevich, S. E. Sharapov, and JET-EFDA Contributors, *Plasma Phys. Controlled Fusion* **46**, S47 (2004).
- <sup>88</sup>R. G. L. Vann, R. O. Dendy, and M. P. Gryaznevich, *Phys. Plasmas* **12**, 032501 (2005).
- <sup>89</sup>M. P. Gryaznevich and S. E. Sharapov, *Nucl. Fusion* **46**, S942 (2006).
- <sup>90</sup>L. Chen, J. Vaclavik, and G. W. Hammett, *Nucl. Fusion* **28**, 389 (1988).
- <sup>91</sup>R. B. White, R. J. Goldston, K. McGuire, A. H. Boozer, D. A. Monticello, and W. Park, *Phys. Fluids* **26**, 2958 (1983).
- <sup>92</sup>D. S. Darrow, E. D. Fredrickson, H. E. Myrick *et al.*, in *Proceedings of the 19th European Conference on Plasma Physics and Controlled Fusion, Innsbruck, 1992* (EPS, 1992), Vol. 16C, Part I, p. 431.
- <sup>93</sup>M. García-Muñoz, H.-U. Fahrbach, S. Günter, V. Igochine, M. J. Manstinen, M. Maraschek, P. Martin, P. Piovesan, K. Sassenberg, and H. Zohm, "Fast ion losses due to high frequency MHD perturbations in the ASDEX Upgrade Tokamak," *Phys. Rev. Lett.* (in press).
- <sup>94</sup>D. J. Sigmar, C. T. Hsu, R. White, and C. Z. Cheng, *Phys. Fluids B* **4**, 1506 (1992).
- <sup>95</sup>K. Nagaoka, private communication (2007).
- <sup>96</sup>H. L. Berk, B. N. Breizman, J. Fitzpatrick, M. S. Pekker, H. V. Wong, and K. L. Wong, *Phys. Plasmas* **3**, 1826 (1996).
- <sup>97</sup>F. Zonca, S. Briguglio, L. Chen, G. Fogaccia, and G. Vlad, *Nucl. Fusion* **45**, 477 (2005).
- <sup>98</sup>E. M. Carolipio, W. W. Heidbrink, C. Z. Cheng, M. S. Chu, G. Y. Fu, A. Jaun, D. A. Spong, A. D. Turnbull, and R. B. White, *Phys. Plasmas* **8**, 3391 (2001).
- <sup>99</sup>Y. Todo, H. L. Berk, and B. N. Breizman, *Phys. Plasmas* **10**, 2888 (2003).
- <sup>100</sup>M. A. Van Zeeland, M. E. Austin, N. N. Gorelenkov, W. W. Heidbrink, G. J. Kramer, G. Y. Fu, M. A. Makowski, G. R. McKee, R. Nazikian, E.

- Ruskov, and A. D. Turnbull, *Phys. Plasmas* **14**, 056102 (2007).
- <sup>101</sup>W. W. Heidbrink, N. N. Gorelenkov, Y. Luo *et al.*, *Phys. Rev. Lett.* **99**, 245002 (2007).
- <sup>102</sup>A. Jaun, K. Appert, J. Vaclavik, and L. Villard, *Comput. Phys. Commun.* **92**, 153 (1995).
- <sup>103</sup>A. Jaun, A. Fasoli, and W. W. Heidbrink, *Phys. Plasmas* **5**, 2952 (1998).
- <sup>104</sup>A. Fasoli, A. Jaun, and D. Testa, *Phys. Lett. A* **265**, 288 (2000).
- <sup>105</sup>J. A. Snipes, N. N. Gorelenkov, and J. A. Sears, *Nucl. Fusion* **46**, 1036 (2006).
- <sup>106</sup>A. Fasoli, D. Testa, T. Panis, A. Klein, J. Snipes, J. Sears, M. Gryaznevich, R. Martin, S. Pinches *et al.*, "Active excitation and damping rate measurement of intermediate-n Alfvén eigenmodes in JET, C-Mod, and MAST," *Nucl. Fusion* (submitted).
- <sup>107</sup>N. A. Crocker, W. A. Peebles, S. Kubota, E. D. Fredrickson, S. M. Kaye, B. P. LeBlanc, and J. E. Menard, *Phys. Rev. Lett.* **97**, 045002 (2006).
- <sup>108</sup>R. Nazikian, H. L. Berk, R. V. Budny *et al.*, *Phys. Rev. Lett.* **96**, 105006 (2006).
- <sup>109</sup>R. Nazikian, private communication (2007).
- <sup>110</sup>W. W. Heidbrink, *Plasma Phys. Controlled Fusion* **9**, 28 (2002).
- <sup>111</sup>M. C. Herrmann and N. J. Fisch, *Phys. Rev. Lett.* **79**, 1495 (1997).
- <sup>112</sup>K. L. Wong, R. Budny, R. Nazikian, C. C. Petty, C. M. Greenfield, W. W. Heidbrink, and E. Ruskov, *Phys. Rev. Lett.* **93**, 085002 (2004).
- <sup>113</sup>M. A. Van Zeeland, W. W. Heidbrink, R. Nazikian *et al.*, "Reversed shear Alfvén eigenmode stabilization by localized electron cyclotron heating," *Plasma Phys. Controlled Fusion* (in press).
- <sup>114</sup>D. Maslovsky, B. Levitt, and M. E. Mauel, *Phys. Rev. Lett.* **90**, 185001 (2003).
- <sup>115</sup>H. Kimura, Y. Kusama, M. Saigusa *et al.*, *Nucl. Fusion* **38**, 1303 (1998).
- <sup>116</sup>D. W. Ross, G. L. Chen, and S. M. Mahajan, *Phys. Fluids* **25**, 652 (1982).
- <sup>117</sup>A. DeChambrier, A. D. Cheetham, A. Heym, F. Hofmann, B. Joye, R. Keller, A. Lietti, J. B. Lister, and A. Pochelon, *Plasma Phys.* **24**, 893 (1982).
- <sup>118</sup>A. Hasegawa and L. Chen, *Phys. Fluids* **19**, 1924 (1976).
- <sup>119</sup>A. Fasoli, D. Borba, B. Breizman, C. Gormezano, R. F. Heeter, A. Jaun, M. Mantsinen, S. Sharapov, and D. Testa, *Phys. Plasmas* **7**, 1816 (2000).
- <sup>120</sup>G. J. Kramer, R. Nazikian, B. Alper *et al.*, *Phys. Plasmas* **13**, 056104 (2006).